

Supporting Information

Hydrogen bond stabilized β -Ni(OH)_x-SO₄ interlaminar materials for highly active supercapacitors

Tingting Li, Shaokang Yang, Yunpeng Zuo, Wei Li, Hongwei Yue, Štěpán Kment, and Yang Chai**

Experimental section

Fig. S1 XRD patterns of Ni₂(CO₃)(OH)₂ and NCO samples.

Fig. S2 XRD patterns of Ni(OH)₂, NSO-0.1, NSO-0.3 and NSO-0.5 samples.

Fig. S3 XRD pattern of clean NSO-0.5 sample.

Fig. S4 Structural refinement results of XRD data for NSO-0.3 sample.

Fig. S5 FESEM images of Ni₂(CO₃)(OH)₂, Ni(OH)₂, NSO-0.1, NSO-0.3, and NSO-0.5 samples.

Fig. S6 SEM images of NCO.

Fig. S7 STEM images of NSO-0.3.

Fig. S8 XPS spectra of NSO-0.3.

Fig. S9 FTIR spectra of Ni₂(CO₃)(OH)₂ and NSO-0.3 samples.

Table S1 EXAFS fitting parameters of various samples.

Fig. S10 GCD curves tested at different current densities.

Fig. S11 CV and GCD curves of NSO-0.3 electrode.

Fig. S12 CV and GCD curves of AC electrode.

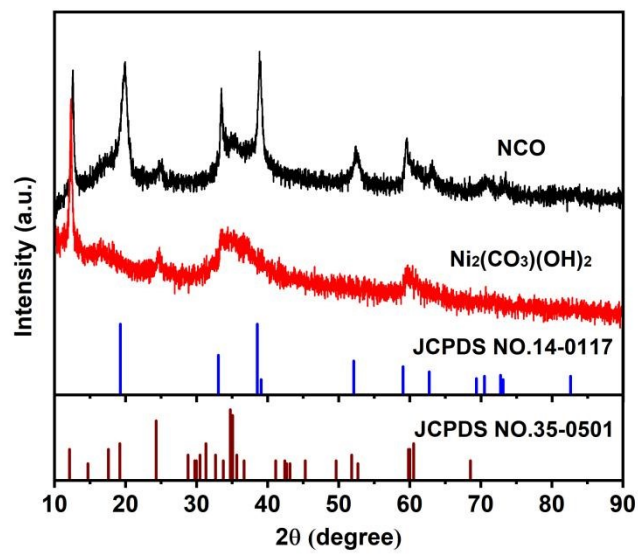


Figure S1. XRD patterns of $\text{Ni}_2(\text{CO}_3)(\text{OH})_2$ and NCO .

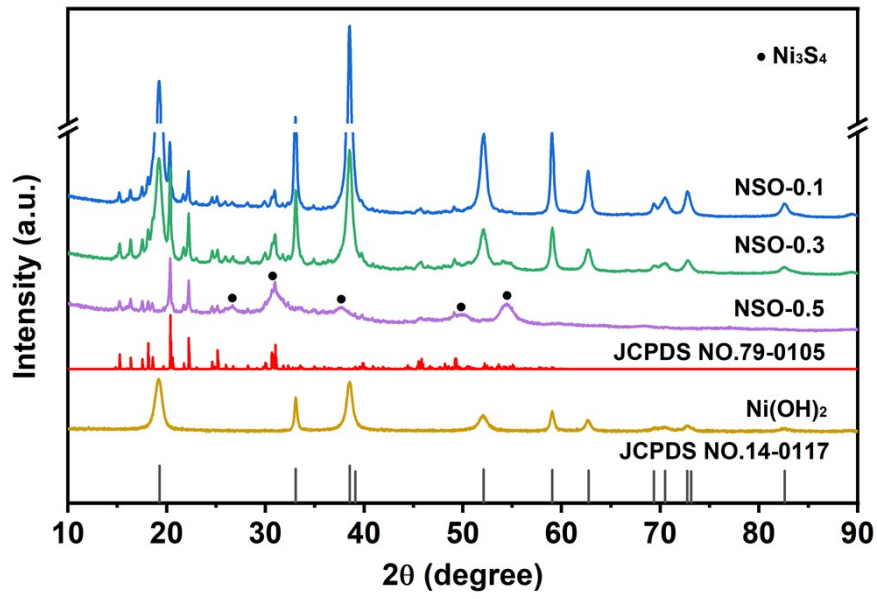


Figure S2. XRD patterns of Ni(OH)₂, NSO-0.1, NSO-0.3 and NSO-0.5.

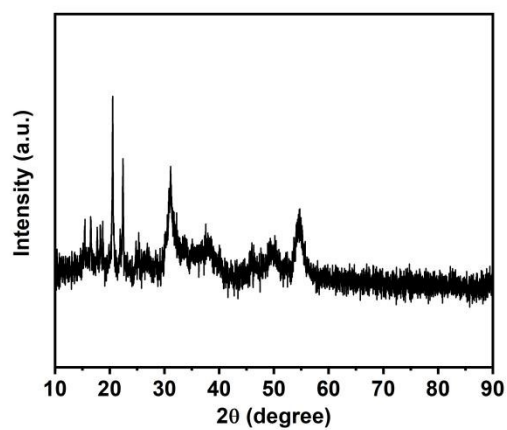


Figure S3. XRD pattern of NSO-0.5 sample with multiple washes.

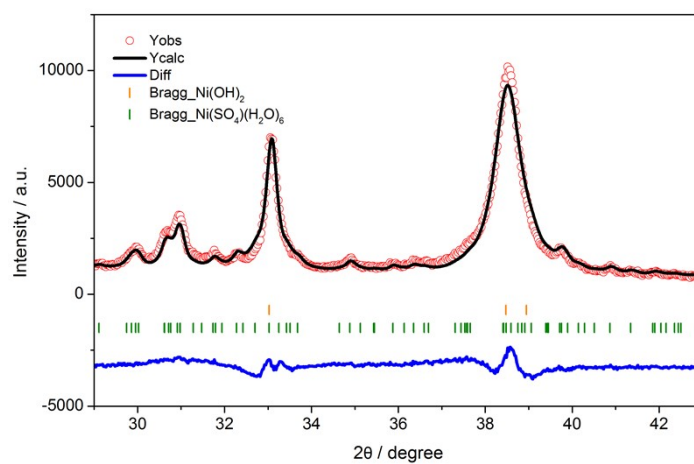


Figure S4. Rietveld refinement of NSO-0.3 sample.

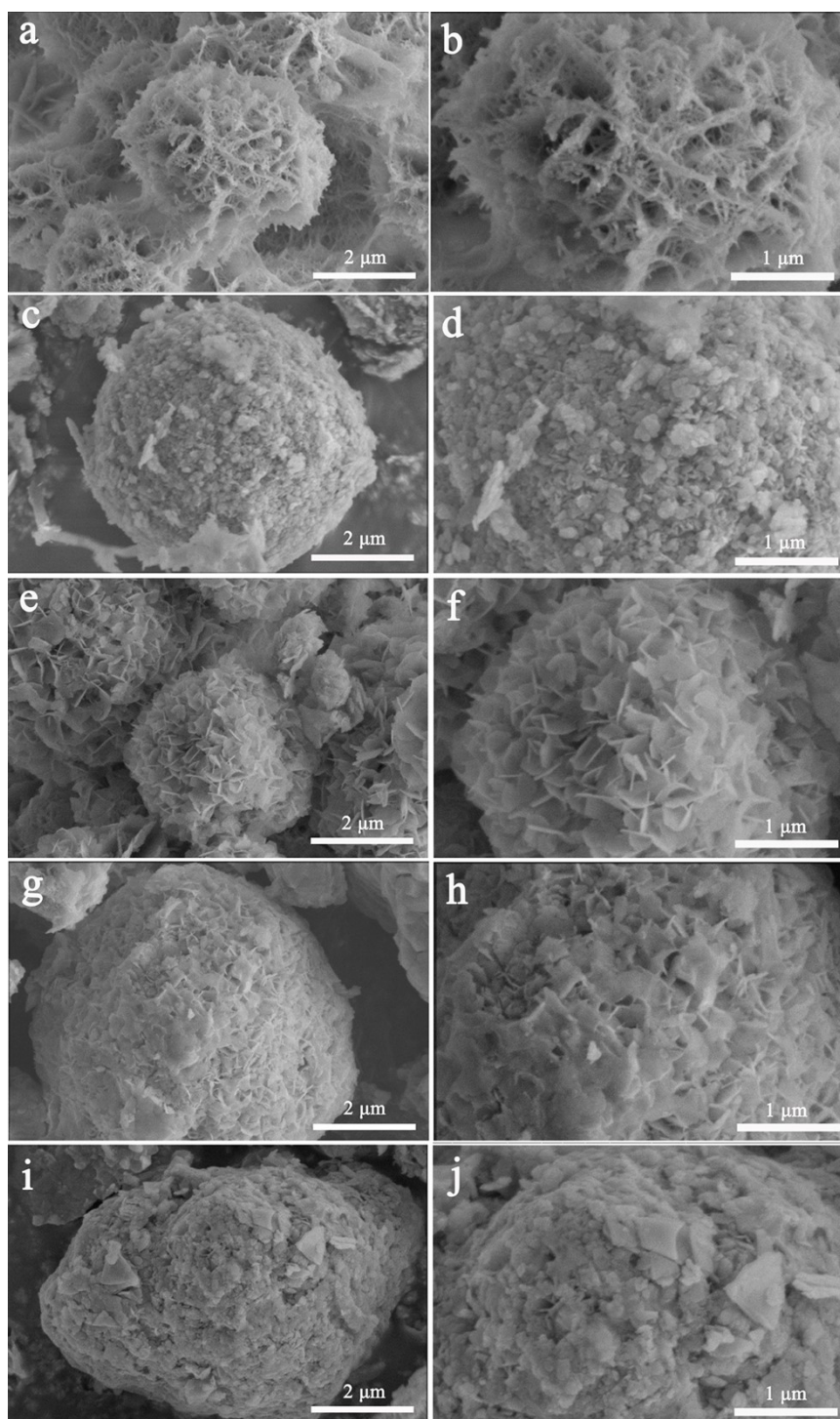


Figure S5. FESEM images of (a, b) $\text{Ni}_2(\text{CO}_3)(\text{OH})_2$, (c, d) $\text{Ni}(\text{OH})_2$, (e, f) NSO-0.1, (g, h) NSO-0.3, and (i, j) NSO-0.5.

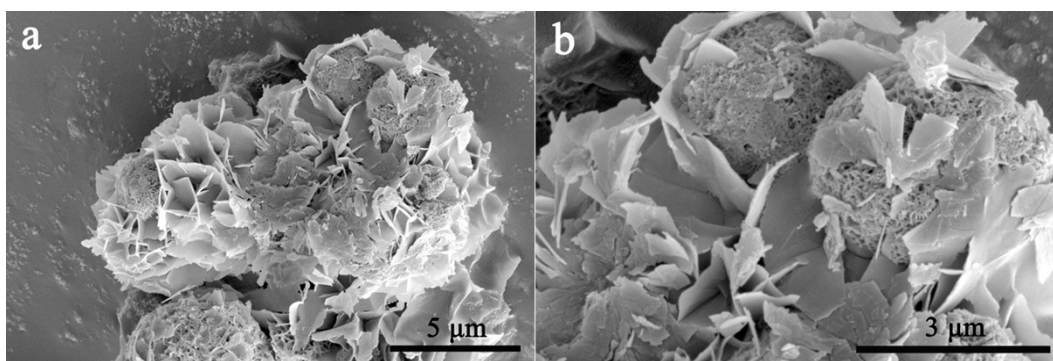


Figure S6. (a, b) Enlarged SEM images of NCO.

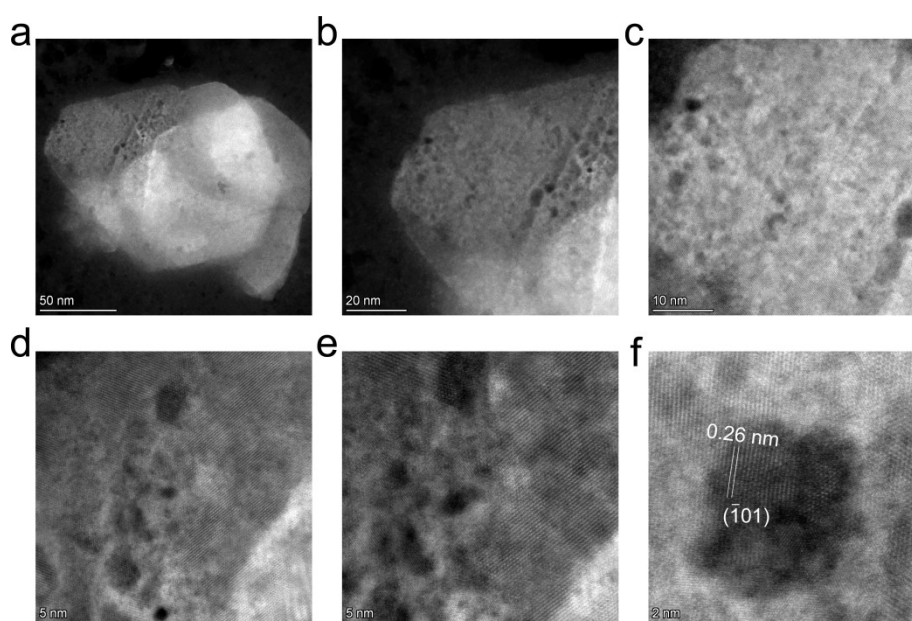
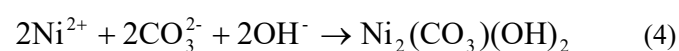


Figure S7. (a-f) Magnified STEM images of representative NSO-0.3 nanosheets. The obtained hybrid materials possess many porous units through the whole structure, providing the 3D accessible of the molecules, which has great application potential for supercapacitors.

Growth mechanism analysis

According to the characterization results, a possible growth mechanism was inferred. $\text{Ni}_2(\text{CO}_3)(\text{OH})_2$ was formed by hydrolysis of urea during the initial hydrothermal process. The involved reactions show in below ^{1,2} :



The $\text{Ni}_2(\text{CO}_3)(\text{OH})_2$ is readily converted to $\beta\text{-Ni}(\text{OH})_2$ due to its thermal instability with subsequent hydrothermal treatment. The morphological evolution from $\text{Ni}_2(\text{CO}_3)(\text{OH})_2$ nanowire to irregular sheet shaped $\beta\text{-Ni}(\text{OH})_2$ in micrometer scale was observed by SEM (Figure S6). The intrinsic growth of $\beta\text{-Ni}(\text{OH})_2$ tends to grow along $\langle 110 \rangle$ direction to form the 2D structure ³. However, the existence of different ions as well as the ion concentration can cause the specific variation in the final morphology ⁴. The added S^{2-} would be oxidized to SO_4^{2-} under the high temperature and pressure ^{5, 6} and the generated SO_4^{2-} anions inserted into the inter-layer of $\text{Ni}(\text{OH})_2$ based on XRD refinement calculation result.

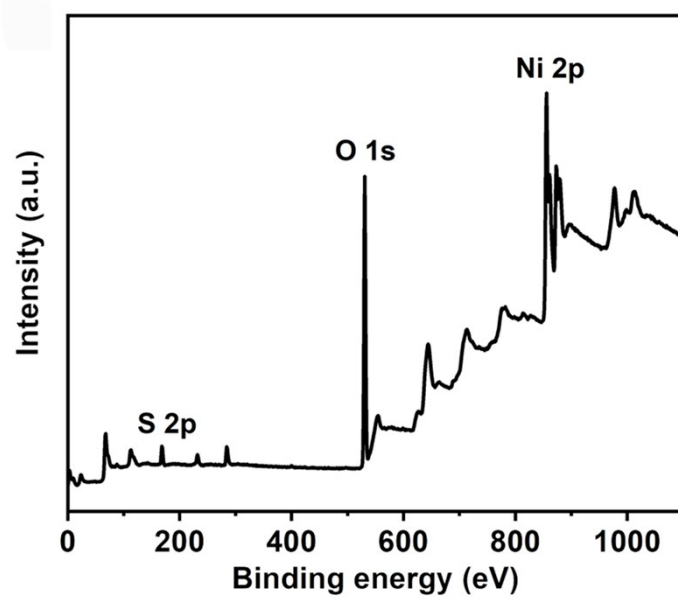


Figure S8. (a) Survey XPS of NSO-0.3.

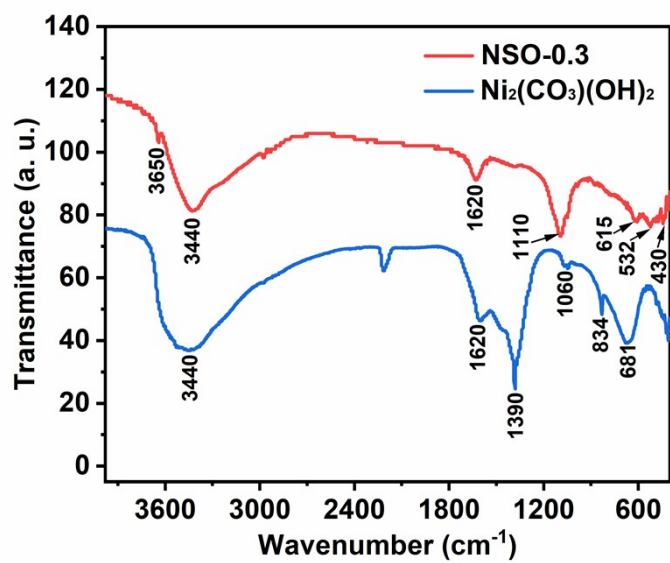


Figure S9. FTIR spectra of Ni₂(CO₃)(OH)₂ and NSO-0.3 samples.

Table S1. EXAFS fitting parameters at the Ni K-edge various samples ($S_0^2=0.79$).

Sample	Path	C.N.	R (Å)	$\sigma^2 \times 10^3$ (Å ²)	ΔE (eV)	R factor
Ni foil	Ni-Ni	12*	2.48±0.01	6.1±0.2	6.6±0.3	0.001
NSO-0.3	Ni-O	1.7±0.3	2.06±0.01	2.8±1.4	2.9±.7	0.018
	Ni-Ni	0.7±0.3	3.07±0.02	2.1±2.9	-4.0±4.7	
Ni(OH) ₂	Ni-O	3.8±0.5	2.06±0.01	3.7±1.1	-2.6±1.9	0.006
	Ni-Ni	4.9±0.8	3.13±0.01	6.7±1.1	-1.9±1.6	

C.N.: coordination numbers; *R*: bond distance; σ^2 : Debye-Waller factors; ΔE : the inner potential correction. *R* factor: goodness of fit. * fitting with fixed parameter.

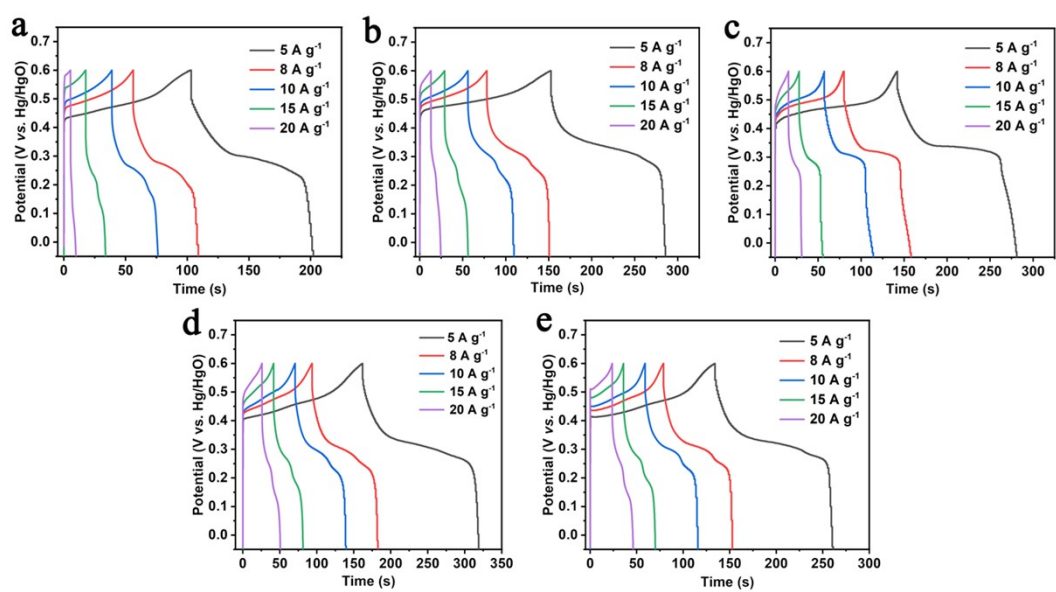


Figure S10. GCD curves tested at different current densities. (a) $\text{Ni}_2(\text{CO}_3)(\text{OH})_2$, (b) $\text{Ni}(\text{OH})_2$, (c) NSO-0.1, (d) NSO-0.3, (e) NSO-0.5.

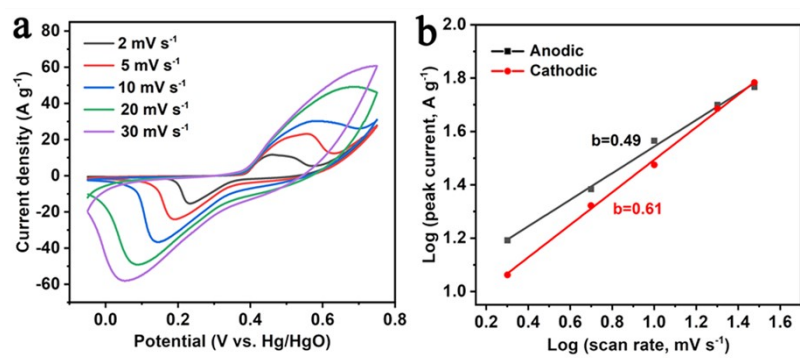


Figure S11. (a) CV curves of NSO-0.3 electrode at different scanning rates, (b) The linear relation between the anodic/cathodic peak current and the scan rates, (c) GCD curves of the NSO-0.3 electrode at different current densities.

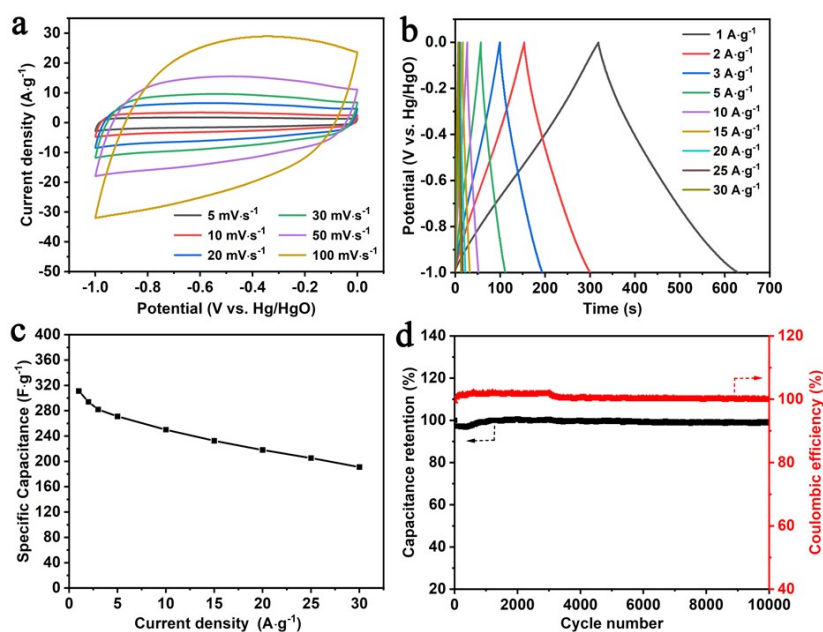


Figure S12. (a) CV and (b) GCD curves of AC electrode. (c) Specific capacitance values of AC electrode plotted against different current densities. (d) Cycling stability and coulombic efficiency of AC electrode.

The electrochemical performance of the activated carbon (AC) electrode is presented in Figure S11. All CV curves exhibited the rectangular shape at scan rate from 5 to 100 mV s⁻¹, indicating the typical electric double layer energy storage mechanism during charge-discharge process. The GCD curves of AC sample showed nearly isosceles triangle (Figure S11b), which confirmed near-ideal electric double layer capacitance behavior. The specific capacitance values were 311, 294, 282, 271, 250, 233, 218, 205 and 191 F g⁻¹ at current density of 1, 2, 3, 5, 10, 15, 20, 25 and 30 A g⁻¹, respectively. Additionally, the AC electrode maintained a high capacitance retention rate of 99.1% and coulomb efficiency of 100.1% after 10,000 charge-discharge cycles at a current density of 5 A g⁻¹. These excellent electrochemical properties reveal the great application potential of AC as a negative electrode for assembling hybrid supercapacitors.

Reference

- [1] G. Zhu, C. Xi, M. Shen, C. Bao, J. Zhu, Nanosheet-based hierarchical $\text{Ni}_2(\text{CO}_3)(\text{OH})_2$ microspheres with weak crystallinity for high-performance supercapacitor. *ACS Appl. Mater. Interfaces* **2014**, *6*, 17208-17214.
- [2] D. Lee, S. Mathur, K. Kim, Bilayered $\text{NiZn}(\text{CO}_3)(\text{OH})_2$ - $\text{Ni}_2(\text{CO}_3)(\text{OH})_2$ nanocomposites as positive electrode for supercapacitors. *Nano Energy* **2021**, *86*, 106076.
- [3] D. Sun, J. Zhang, H. Ren, Z. Cui, D. Sun, Influence of OH^- and SO_4^{2-} anions on morphologies of the nanosized nickel hydroxide. *J. Phys. Chem. C* **2010**, *114*, 12110-12116.
- [4] H. Wang, Y. Chen, L. Wan, Y. Deng, W. Hu, Hydrothermal synthesis, characterisation and growth mechanism of $\text{Ni}(\text{SO}_4)_{0.3}(\text{OH})_{1.4}$ nanowires. *Micro & Nano Letters* **2015**, *10*, 567-572.
- [5] X. Zhang, F. Jia, B. Yang, S. Song, Oxidation of molybdenum disulfide sheet in water under in situ atomic force microscopy observation. *J. Phys. Chem. C* **2017**, *121*, 9938-9943.
- [6] L. Zheng, Z. Liu, K. Xie, W. Ma, K. Wei, Thermodynamic research of S-H₂O system in sodium aluminate solution. *Key Eng. Mater.* **2017**, *730*, 272-281.